

Monodisperse platinum nanoparticles of well-defined shape: synthesis, characterization, catalytic properties and future prospects

R.M. Rioux^a, H. Song^{a,b}, M. Grass^a, S. Habas^a, K. Niesz^a, J.D. Hoefelmeyer^{a,c}, P. Yang^{a,*}, and G.A. Somorjai^{a,*},

^aDepartment of Chemistry, University of California, Berkeley and Materials Sciences Division, Lawrence Berkeley National Laboratory, Berkeley, CA 94720, USA

^bDepartment of Chemistry, Korea Advanced Institute of Science and Technology, Daejeon, 305-701, Korea

^cDepartment of Chemistry, University of South Dakota, Vermillion, SD 57069, USA

Monodisperse platinum nanoparticles with well-defined faceting have been synthesized by a modified polyol process with the addition of silver ions. Pt nanoparticles are encapsulated in mesoporous silica during *in situ* hydrothermal growth of the high surface area support. Removal of the surface regulating polymer, poly(vinylpyrrolidone), was achieved using thermal oxidation-reduction treatments. Catalysts were active for ethylene hydrogenation after polymer removal. Rates for ethylene hydrogenation decreased in accordance with the amount of Ag retained in the Pt nanoparticles after purification. Ag is most likely present on the Pt particle surface as small clusters. Future prospects for these catalysts for use in low temperature selective hydrogenation reactions are discussed.

KEY WORDS: nanoparticle synthesis; particle shape; catalyst characterization; reaction selectivity.

1. Introduction

The surface structure of small metal crystallites changes most dramatically in the 1–5 nm size range and in the case of some reactions catalytic activity is sensitive to particle size changes in this regime [1–6]. As crystal domains become smaller, the ratio of corner and edge atoms to terrace atoms increases [7–10] and the surface topology becomes increasingly roughened. Dimensional control of particles and resulting changes in surface and electronic states, presents an opportunity to tailor particle surfaces to affect substrate interactions. Substrate adsorption on corner and edge atoms, that possess open coordination spheres, can be significantly different, in terms of bond enthalpies, desorption energies, and adsorption geometry, than adsorption occurring on terrace sites. An illustrative example of this concept is the dissociation of CO on Rh surfaces, which is nine orders of magnitude faster on Rh(211) than Rh(111), due to the presence of exposed sites on the step edges of Rh(211) that do not exist on Rh(111) [11].

Boudart has classified catalytic reactions whose rate varies as a function of particle size as structure sensitive [12]. Significant advances in understanding catalytic phenomena, such as the concept of structure sensitive/insensitive reactions, are the result of studying such phenomena on model catalytic systems [13]. The most recent extension of model catalytic systems, or at the very least the simplification of a complex supported catalyst, is the synthesis of monodisperse transition

metal nanoparticles with uniform size and shape and their incorporation into high surface area oxide support matrices [14–17]. The materials are intended as three dimensional model catalysts, where particle characteristics, such as size, shape, or crystallinity, are controllably varied to probe for influence on catalytic activity and selectivity [15,16,18–21]. Solution syntheses of Pt particles yield monodisperse samples with tunable size and shape. Catalyst materials that are prepared by the combination of the proper support and monodisperse particles have unprecedented uniformity, which is difficult to achieve with conventional catalyst synthetic methods.

The effect of metal nanoparticle size on catalytic activity is better understood than the influence of nanoparticle shape on catalytic activity, since size control of crystallites has generally been easier to achieve than shape control.

Introduction of foreign ions during solution phase synthesis of metal nanoparticles is a major parameter for controlling particle shape. Xia *et al.* have extensively studied morphology changes of noble metal nanoparticles (Ag, Pd, and Pt) by adding various foreign ions [22]. They observed that chloride ions and oxygen in the reaction mixture preferentially dissolved twinned particles initially formed during reduction and led to selective formation of single crystalline products such as truncated tetrahedra and cuboctahedra. In another study by Xia *et al.* [23], trace amounts of iron chloride slowed the reduction of Pt(II) species, inducing optimal anisotropic growth condition during a polyol process to form agglomerates of single-crystalline Pt nanowires rather than small (<5 nm) Pt crystallites which formed

* To whom correspondence should be addressed.

E-mails: p_yang@berkeley.edu; somorjai@berkeley.edu

without iron chloride. The addition of large amounts of NaNO_3 to a Pt salt solution led to the formation of branched nanostructures due to platinum nitrate formation, which alters the reduction kinetics of Pt [24]. Addition of silver ions in a polyol synthesis of Pt nanoparticles results in lower nucleation temperatures, which favor anisotropic growth to form Pt multipods [25]. Although several foreign ions have been reported to substantially affect particle morphologies, the exact mechanism has not been determined. It is thought that selective adsorption of the additive ion on one or more crystal surfaces changes the selective growth rate of crystal faces leading to the change of shape [26].

Previously, we demonstrated the synthesis of Pt nanocrystals of well-defined shape (cubes, octahedra, and cuboctahedra) using silver ions [27] and poly(vinylpyrrolidone) (PVP) in solution. In this paper, we demonstrate their encapsulation in mesoporous silica (SBA-15) during in-situ hydrothermal growth. Physical and chemical properties are determined and the prospect of these catalysts serving as models of complex technical catalysts is discussed. The study of reaction selectivity during the hydrogenation of α,β unsaturated aldehyde is suggested as a probe of nanoparticle surface structure.

2. Experimental

2.1. Nanoparticle synthesis

A detailed description of the synthesis of the nanoparticles has been published elsewhere [27]. A brief description of the synthesis is given here. Synthesis of Pt cubes began with the introduction of 0.5 mL of 2×10^{-3} M silver nitrate (AgNO_3 , 99+%, Sigma-Aldrich) solution in ethylene glycol (EG) to boiling EG followed by the immediate introduction of 3 mL of poly(vinylpyrrolidone) (PVP, MW = 55 K, Sigma-Aldrich, 0.375 M) and 1.5 mL of hexachloroplatinic acid ($\text{H}_2\text{PtCl}_6 \cdot 6\text{H}_2\text{O}$, 99.9%, metals basis, Alfa-Aesar, 0.0625 M) EG solutions dropwise over 16 min. The resulting mixture was heated at reflux for an additional 5 min followed by centrifugation. After separation of the supernatant and precipitate in acetone, the precipitate was redispersed and washed with ethanol twice and finally dispersed in ethanol. Increasing the molarity of the AgNO_3 solution to 2×10^{-2} M and 6×10^{-2} M led to the selective formation of cuboctahedral and octahedral particles, respectively.

2.2. Catalyst synthesis and characterization

A detailed procedure for the synthesis of catalysts by nanoparticle encapsulation (NE) in high surface area mesoporous silica can be found elsewhere [28]. A brief description is given here. A Pt colloid aqueous solution (27.0 mL, 3×10^{-3} M) was mixed with 50.5 mL of aqueous polymer solution (Pluronic P123, $\text{EO}_{20}\text{PO}_{70}\text{EO}_{20}$,

EO = ethylene oxide, PO = propylene oxide, BASF, 2.5 g) and stirred for 1 h at 313 K followed by the quick addition of 0.375 mL of 0.5 M sodium fluoride (NaF, 99.99%, Aldrich) aqueous solution and 3.91 mL of tetramethyl orthosilicate (TMOS, 98%, Aldrich) to the reaction mixture, followed by stirring for a day at 313 K. The resulting slurry was aged for an additional day at 373 K. The brown precipitate was separated by centrifugation, thoroughly washed with ethanol, and dried in an oven at 373 K.

Elemental analysis of the catalysts for Pt and Ag content were determined by inductively coupled plasma-atomic emission spectroscopy (ICP-AES) at Galbraith Laboratories Inc. (Knoxville, TN). Catalysts were made to have a nominal weight loading of 1% Pt; actual loadings ranged from 0.5–0.7% by weight as determined by ICP-AES. XRD diffractograms of the supported Pt catalysts were measured on a Bruker D8 GADDS diffractometer using $\text{Co K}\alpha$ radiation (1.79 Å) and the particle size was calculated by the Scherrer equation. Catalysts used for ethylene hydrogenation were calcined in 20% O_2/He (total flow 50 cc (STP) min^{-1}) for 1 h at 473 K, purged with He for $\frac{1}{2}$ h at 473 K, followed by reduction in H_2 (50 cc (STP) min^{-1}) for 1 h at 473 K. Cyclic oxidation-reduction experiments confirmed that ethylene hydrogenation activity was maximized after one treatment cycle [29].

2.3. Reactivity studies: ethylene hydrogenation as a surface probe

Catalytic reactions were studied in a Pyrex plug flow reactor connected to a 1/4 stainless steel tubing manifold containing mass flow controllers (Unit Instruments) for delivery of reactant gases. Ethylene (AirGas, CP grade), hydrogen (Praxair, UHP, 99.999%) and helium (Praxair, UHP, 99.999%) were used as received. Reaction temperatures were measured with a thermocouple extending into the catalyst bed. Reactants and products were detected by gas chromatography (Hewlett Packard 5890) and quantified using Dietz tables [30]. Reaction rate measurements were conducted at differential conditions (all conversions, $X < 10\%$). Catalysts (5–15 mg) were diluted with low surface area acid washed quartz in a 1:3 ratio (catalyst:quartz). The Madon–Boudart test [31] verified the absence of heat and mass transfer limitations.

3. Results and discussion

3.1. Nanoparticle and catalyst synthesis

The results for both nanoparticle [27] and catalyst syntheses [28] have been previously published. Details of both syntheses are summarized here. The slow addition of separate PVP and $\text{H}_2\text{PtCl}_6 \cdot 6\text{H}_2\text{O}$ solutions to boiling EG caused the color of the solution to change from

yellow to dark brown indicating the fast reduction of Pt(IV) species to Pt(0) species. If Ag ions were not added prior to the introduction of the Pt salt, a distribution of Pt particle shapes were obtained [27]. Only upon addition of varying concentrations of AgNO_3 is preferential growth of the Pt nanoparticles observed. At a AgNO_3 concentration of 1.1 mol% (relative to Pt salt concentration), cubes are formed with $\sim 80\%$ selectivity (figure 1(a)), while at 11% and 32 mol% AgNO_3 , cuboctahedra and octahedra are synthesized with $\sim 100\%$ and 80% selectivity, respectively (figure 1(b) and (c)). In the case of cube and octahedra synthesis, the minor shape is tetrahedral. In all cases, the largest vertex-to-vertex distance is ~ 9.5 nm ($\sigma \sim 7\%$) regardless of shape. Size and shape of the as-synthesized particles were dependent upon the addition rate of PVP and $\text{H}_2\text{PtCl}_6 \cdot 6\text{H}_2\text{O}$. A single addition led to the formation of 4 nm particles with no dominant shape, while slow addition (over 30 min time period) led to polycrystalline particles with diameters ≥ 13 nm. It was determined that the addition of PVP and Pt salt over a 16 min time period was optimal. A summary of the Pt particle shapes and yield is shown in Table 1. Cubes and octahedra are terminated entirely by (100) and (111) planes, respectively, while cuboctahedra are terminated by eight (100) and six (111) surfaces.

UV-Vis absorption spectroscopy under synthetic conditions in the presence of Ag ions suggested the presence of reduced Ag_4^{2+} species during the early stages of synthesis; with the formation of Ag particles at longer synthesis times [27]. It is believed that the mechanism for Pt nanoparticle growth involves enhanced growth along $\langle 100 \rangle$ and/or suppressed growth along $\langle 111 \rangle$ due the introduction of Ag ions and their strong adsorption on $\{100\}$ terminated Pt

surfaces. The growth of Ag thin films on single crystalline Pt surfaces has shown that the desorption activation energy of Ag on Pt(100) is higher than on Pt(111) [31]. Some of the silver is removed by repetitive centrifugation and dispersion after Pt particle formation as determined by UV-Vis spectroscopy [27]. This work represents one of the first reports of control over both nanoparticle size and shape under the same synthesis conditions [27].

After purification of the Pt nanoparticles, they were introduced into an aqueous solution of Pluronic P123. In a typical reaction, a Pt colloid solution was mixed with the aqueous polymer solution at 313 K, and stirred for 1 h to ensure complete dispersion of the Pt particles. Brown precipitates were formed in 5 min after the addition of NaF solution and TMOS. The supernatant was colorless and transparent, indicating that all Pt colloids were incorporated into the silica matrix. The slurry was aged for a day at 313 K and placed in an oven at 373 K for an additional day. The product was washed with water and ethanol, and dried in air at 373 K. Figure 2 shows a schematic of the NE method and a TEM micrograph of the 0.55% Pt(cubes)/SBA-15 catalyst. The Pt particles are isolated and located within the silica framework without severe aggregation. This method has been successfully utilized with PVP capped monodispersed Pt nanoparticles ranging in size from 1.7–7.1 nm [28].

Removal of PVP or any other surface stabilizing polymer represents a significant challenge. In most circumstances, these organic molecules are bound strongly to the nanoparticle surface at approximately monolayer coverage. Thermal degradation or calcination of the adsorbed organics are two possible methods for removal and cleansing of the Pt surface. These methods generally

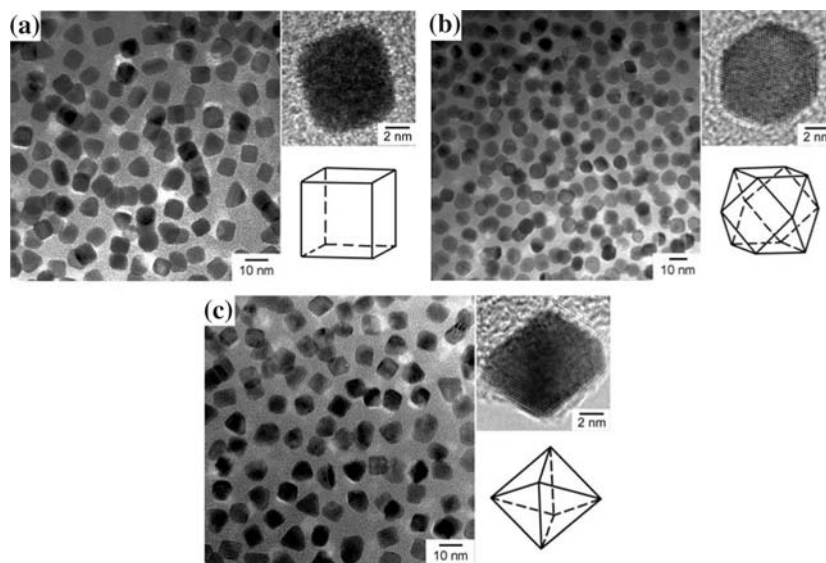


Figure 1. TEM micrograph of as-synthesized Pt nanoparticles with distinct shapes: (a) cubes, (b) cuboctahedra and (c) octahedra. Inset: HRTEM image and ideal structure of major particle shape. Partly adapted from reference [27].

Table 1
Yield and average size of Pt nanoparticles^a

Amount of Ag added ^b	Major shape yield ^c and average size ^d	Minor shape yield ^c and average size ^d
0 mol%	Cubes with rounded edges ~40%	Spheres, ~30% Irregular rods, ~20% Tetrahedra, ~10%
1.1 mol%	Cubes ~80%, 9.4 ± 0.6 nm	Tetrahedra ~10%, 9.8 ± 0.7 nm
11 mol%	Cuboctahedra ~100%, 9.1 ± 0.6 nm	–
32 mol%	Octahedra ~80%, 9.8 ± 0.6 nm	Tetrahedra ~10%, 9.9 ± 0.7 nm

^aReproduced from reference [27].

^bWith respect to the Pt salt concentration.

^cStatistically determined values based on counting 250 particles.

^dLargest vertex to vertex distance.

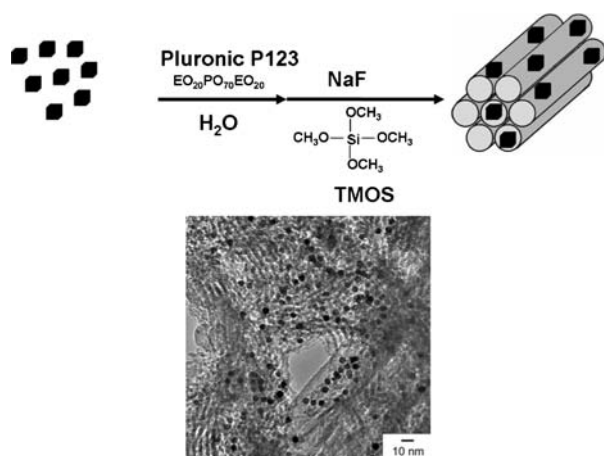


Figure 2. Scheme for nanoparticle encapsulation (NE) synthesis of Pt/SBA-15 catalysts and TEM micrograph of a 0.55% Pt(cubes)/SBA-15 catalyst.

require high temperatures and local hot spots can be generated at the nanoparticle surface during calcination. In this study, hot spots were avoided by calcination in dilute oxygen (20% O₂/He, Praxair, UHP both gases). Thermal gravimetric analysis of unsupported Pt cubes demonstrates that calcination is much more effective for PVP removal than thermal treatment in N₂ (figure 3(a)). PVP decomposes at 473–623 K under O₂ flow; 150 K lower than with N₂. Figure 3(b) demonstrates that free PVP decomposes at ~600 K. Pt apparently catalyzes the combustion of PVP by the diffusion of O₂ through the randomly tangled alkyl chains of PVP and dissociation on a clean ensemble of Pt atoms, whereupon catalytic decomposition occurs. Isothermal treatments of free PVP and PVP-Pt/SiO₂ physical mixtures in inert (He) and reactive (oxygen) atmospheres confirm that O₂ is more effective toward PVP degradation, and clean Pt catalyzes PVP decomposition at 523 K [29]. While thermal treatments in N₂ or He are effective for removing PVP, both require relatively high temperatures. In-situ vacuum transmission electron microscopy imaging of these same nanoparticles adsorbed to amorphous silica grids at temperatures up to 1073 K demonstrate that Pt nanoparticles become truncated

at ~623 K, then spherical and finally the particles spread on the support as the temperature increases [32]. These temperatures are close to those required to remove PVP from the nanoparticle surface. Recently, it has been shown that cyclic oxidation-reduction treatments are effective for removal of PVP with each cycle removing more surface bound PVP or carbon as indicated by ethylene hydrogenation reaction rates [29]. Most of the PVP is removed by calcination at 473 K as determined by infrared spectroscopy, thermal gravimetric analysis and temperature programmed oxidation [29].

3.2. Characterization and ethylene hydrogenation studies of Pt/SBA-15 catalysts

Elemental analyses (Table 2) of the Pt/SBA-15 catalysts by ICP-AES showed that Pt loadings were in the range of 0.5 – 0.7 wt.%. Ag residues were also present in the nanoparticles. Ag components such as Ag(0) and AgCl were not found in previous XRD and Energy Dispersive X-ray spectroscopy (EDX) studies on thoroughly washed small sample batches [27]. It has proven difficult to remove silver completely from large sample batches necessary for catalyst preparation, quantitative elemental analyses showed that Ag residues were actually present at levels corresponding to Ag/Pt molar ratios of 0.014, 0.102, and 0.123 for the cubes, cuboctahedra, and octahedra, respectively, based on the Pt and Ag content reported in Table 2. The exact nature of such silver species and their location (i.e. whether on Pt surface or embedded within PVP coating) are unknown at this point. If imbedded within the PVP coating it is believed that upon calcination and PVP removal, Ag is subsequently deposited on the Pt nanoparticle surface.

BET N₂ adsorption measurements were carried out on the Pt/SBA-15 catalysts and summarized in Table 2. The surface areas of the catalysts are ~500 m² g⁻¹, slightly lower than pristine SBA-15 [28]. The pore volumes are in the range of ~1.9 cc (STP) g⁻¹, and the average pore diameters calculated from desorption branches are around 9 nm. Table 2 contains the Pt

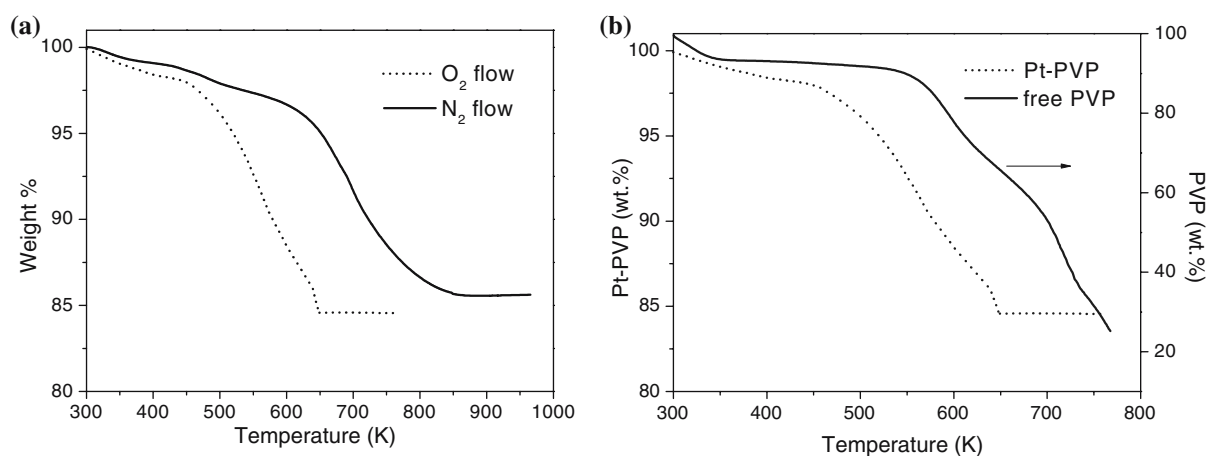


Figure 3. Thermogravimetric analysis (TGA) of (a) influence of thermal treatment atmosphere on PVP decomposition from Pt cubes and (b) oxidative decomposition of free PVP and PVP capped Pt cubes.

Table 2
Elemental analysis and physical properties of Pt/SBA-15 catalysts

Catalyst	Pt loading ^a (wt. %)	Ag loading ^a (ppm)	Physisorption parameters			XRD particle size ^c (nm)
			BET surface area (m ² g ⁻¹)	BJH pore size (Å)	Pore volume (cc (STP) g ⁻¹) ^b	
Pt(cubes)/SBA-15	0.55	43	498	9.0	1.86	7.5
Pt(cuboctahedra)/SBA-15	0.67	378	505	9.2	1.78	8.4
Pt(octahedra)/SBA-15	0.48	326	511	9.3	1.90	8.9

^aDetermined by inductively coupled plasma atomic emission spectrometry (ICP-AES).

^bBased on the Kelvin equation at $P/P_0 = 0.975$.

^cBased on the Scherrer equation.

particle size determined by line-broadening techniques using the Scherrer equation. Measured XRD particle sizes agree with previous results [27].

Rates of ethylene hydrogenation were measured at low conversions over all catalysts. Initial specific rates for ethylene hydrogenation varied from ~ 0.1 to $37 \mu\text{mol g}^{-1} \text{s}^{-1}$, while turnover frequencies (TOF, s^{-1}) differed by three orders of magnitude over the three catalysts (Table 3). The cubes, with the lowest level of Ag incorporation (Table 2) had the highest rate ($\sim 9 \text{s}^{-1}$), in good agreement with measurements on Pt(111) [33] and other types of Pt catalysts [28,33–41] (Table 4). Turnover frequencies reported in Table 4 vary from 1 to 10s^{-1} confirming that the rate measured over pure Pt catalysts with very different morphologies (i.e. single crystals and supported nanoparticles) are similar. In a comprehensive study of the influence of particle size on ethylene hydrogenation, Dorling *et al.* found that the areal rate was invariant with particle size [38]. Based on the above observations, when normalized to the Pt surface area or the number of surface Pt atoms, ethylene hydrogenation rates on the three Pt nanoparticle shapes should be similar. In fact, Pt nanoparticles with higher levels of Ag incorporation are much less active for ethylene hydrogenation on a per surface Pt

atom basis; the TOF decreased to 0.4 and $2 \times 10^{-2} \text{s}^{-1}$ for the cuboctahedra and octahedra, respectively. These reported turnover rates are nominal and represent a minimum because all surface atoms were assumed platinum. Hydrogenation of ethylene on Ag/SiO₂ catalysts does not occur until temperatures $\geq 550 \text{K}$ and Ag is only active if highly dispersed [42]; bulk Ag powder was inactive for ethylene hydrogenation at 300 K [43]. The reduction in rate is associated with the presence of Ag present on the surface of the Pt nanoparticles as small clusters which most likely modify the electronic structure of Pt, as recently shown for a bimetallic Pt–Cu/SiO₂ catalyst [44,45]. Camprostrini *et al.* studied the hydrogenation of propylene over a series of Pt–Ag/SiO₂ alloy catalysts with Pt/Ag molar ratio ranging from 0.83 to 0.12; the authors found the olefin hydrogenation specific rate decreased substantially as Ag content increased and kinetic parameters such as reaction orders and activation energy changed as more Ag was introduced [46]. Pure Pt catalysts were ~ 50 times more active than a Pt–Ag catalyst with Pt/Ag ratio of 0.12. These catalysts have Ag loadings much greater than those used in this study, but confirm Ag influences olefin hydrogenation on Pt catalysts. Adsorption and infrared studies of probe gases (H₂, O₂, CO) on Pt–Ag alloy

Table 3
Kinetics of ethylene hydrogenation on Pt/SBA-15 catalyst series

Catalyst ^a	Activity ^b ($\mu\text{mol g}^{-1} \text{s}^{-1}$)	Turnover frequency ^{b,c} (s^{-1})	E_a^d (kcal mol ⁻¹)
0.55% Pt(cubes)/SBA-15	36.6	8.6	9.9
0.67% Pt(cuboctahedra)/SBA-15	1.9	0.4	10.8
0.48% Pt(octahedra)/SBA-15	0.07	2×10^{-2}	13.4

^aCatalysts were pretreated in 20% O₂/He for 1 h followed by reduction in H₂ for 1 h at 473 K.

^bReaction conditions were 10 Torr C₂H₄, 100 Torr H₂, and 298 K.

^cNormalized to the number of surface atoms using the following relationship, $D = 1.13/d$ (nm) where D is the dispersion and d is the particle diameter determined by XRD.

^dReaction conditions were 10 Torr C₂H₄, 100 Torr H₂ and 273–373 K (catalyst dependent).

Table 4
Comparison of ethylene hydrogenation rates on various types of Pt catalysts

Catalyst	Ethylene turnover frequency (TOF) ^a (s^{-1})	Reference
Pt(111)	9.3	34
Pt(100)-(5×20)	3.6	35
Pt(210)	7.8	36
Pt nanoparticle array/Al ₂ O ₃	6.5	37
Pt nanoparticle array/SiO ₂	4.7	38
~0.7% Pt(X)/SBA-15 (X = 1.7, 2.9, 3.6 or 7.1 nm)	3.5	28
2.45% Pt/SiO ₂	9.3	39
0.05% Pt/SiO ₂	1.3	40
Pt wire	3.0	41
0.04% Pt/SiO ₂	4.4	42

^aCorrected to standard conditions of 10 Torr C₂H₄, 100 Torr H₂ and 298 K.

nanoparticles supported on SiO₂ suggest that Pt does not segregate to the surface under reducing conditions, while oxidizing conditions leads to segregation of Ag to the surface for catalysts with Ag atomic compositions as high as 64% [47]. It is worth noting that the pretreatment of all catalysts in this study included a 1 h oxidation step. Ag incorporation in the cuboctahedra and octahedra was significantly higher than in the cubes, suggesting that Ag may be located on the particle surface or a few atomic layers below surface. Ag is believed to be present on the surface because XRD measurements do not indicate the formation of a PtAg alloy, consistent with their complete immiscibility in the bulk [48]. Lahiri *et al.* [49] have shown that Pt and Ag do not alloy at the nanoscale (2 nm Pt core particle), but rather form Ag–Pt coreshell nanoparticles. The deposition and growth of Ag adlayers on Pt(111) leads to monolayer confined mixing, i.e. Ag is confined to the topmost layer [50,51]. Mixing at the Pt–Ag interface occurs at step edges and Ag is present as small clusters at submonolayer Ag coverages [51]. Based on the observed kinetic results and previous studies of bimetallic Ag–Pt particle synthesis and thin film growth, it is believed that Ag residues are present on the Pt particle surface in the case of the cuboctahedra and octahedra.

3.3. Future prospects: influence of surface structure on reaction selectivity

The ability to synthesize monodisperse Pt nanoparticles of catalytically relevant size (≤ 10 nm) with well-defined shape is a significant achievement in the development of a supported model catalyst. Our agenda with regards to these well-defined nanoparticle/silica catalysts is to study the influence of surface structure on catalytic reaction selectivity. Low temperature (≤ 400 K) multi-path reactions have been targeted due to the instability of the nanoparticle surface structure above ~ 573 K as demonstrated by electron microscopy [32]. A likely prototype reaction for this type of study is the hydrogenation of α,β unsaturated aldehydes; acrolein (C₃H₄O), crotonaldehyde (C₄H₉O) and cinnamaldehyde (C₉H₈O). Acrolein and crotonaldehyde have proven more difficult to selectively hydrogenate than cinnamaldehyde [52].

Selective hydrogenation of the carbonyl group in acrolein and crotonaldehyde is very difficult and with many catalysts both the C=C and C=O bonds are hydrogenated to yield the primary alcohol. Selective formation of the allylic alcohols is preferred because they are valuable intermediates for the production of perfumes and pharmaceuticals [52]. The reaction scheme for crotonaldehyde hydrogenation is shown in figure 4(a). Reported selectivities to crotyl alcohol for SiO₂ supported Pt catalysts are generally low ($\leq 10\%$), but selectivities as high as 43% have been reported for Pt/SiO₂ catalysts with no additives [53–55]. Santori *et al.* [54] have shown that the selectivity to crotyl alcohol during liquid phase crotonaldehyde hydrogenation increases from 9% to 35% at 80% conversion as the Pt particle size on SiO₂ and Al₂O₃ supported catalysts increases from 2 to 6 nm.

Higher selectivity to crotyl alcohol on catalysts containing larger Pt particles suggest that low index faces of fcc metals such as Pt(111) are required for C=O hydrogenation rather than open, low coordination step and kink sites which facilitate hydrogenation of both C=C and C=O bonds [56,57]. Theoretical results of crotonaldehyde adsorption and hydrogenation have

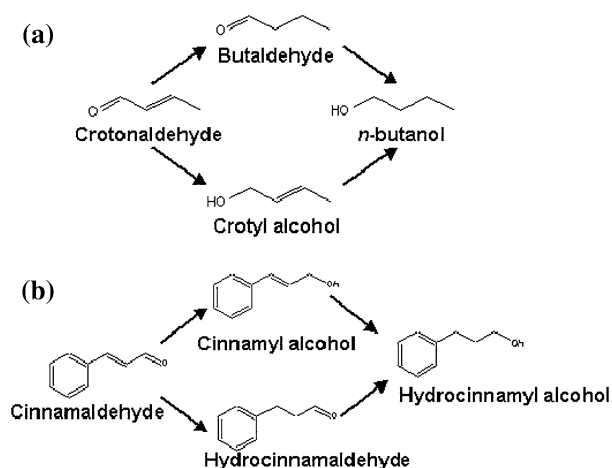


Figure 4. Reaction scheme for hydrogenation of α,β unsaturated aldehydes: (a) crotonaldehyde and (b) cinnamaldehyde.

shown hydrogenation of the carbonyl bond is preferred on Pt(111) over other Pt single crystal surfaces [58,59].

A low temperature reaction involving the hydrogenation of an aromatic α,β unsaturated aromatic aldehyde, cinnamaldehyde is similarly suited for a study of selectivity versus surface structure. The reaction scheme is shown in figure 4(b). As in the case of crotonaldehyde hydrogenation, the unsaturated alcohol is the favored product. Gallezot and co-workers have shown the selectivity to cinnamyl alcohol from cinnamaldehyde has a strong dependence on Pt particle size. The selectivity to the alcohol varied from 83% to 98% (at 50% conversion) as the particle size was increased from 1.3 to ~ 5 nm [60]. The increased selectivity of larger particles is attributed to a steric repulsion between the flat metal surface and aromatic ring causing hindered adsorption and preferential hydrogenation of the carbonyl group [60,61]. Crotonaldehyde and cinnamaldehyde hydrogenation may serve as probe reactions of the Pt nanoparticle surface structure because the (111) surface is more selective for the formation of the unsaturated alcohol. The fraction of exposed (111) faces is greatest in the octahedra (and tetrahedra) followed by the cuboctahedra while cubes are terminated on all sides by (100) surfaces.

4. Conclusions

The synthesis of ~ 9 nm Pt nanoparticles of well-defined shape with the use of silver ions and surface templating polymers in protic solvents has been demonstrated. Addition of increasing amounts of AgNO_3 to refluxing EG followed by slow introduction of $\text{H}_2\text{PtCl}_6 \cdot 6\text{H}_2\text{O}$ led to the formation of cubes, cuboctahedra and octahedra with shape uniformity greater than eighty percent. The Pt nanoparticles are incorporated into a mesoporous silica matrix by hydrothermal growth and encapsulation in aqueous solution.

Removal of the surface templating polymer was achieved with thermal oxidation-reduction treatments. The catalysts are active for ethylene hydrogenation and are promising materials for future studies on the influence of catalyst particle shape on reaction selectivity during the low temperature hydrogenation of α,β unsaturated aldehydes.

Acknowledgments

This work was supported by the Director, Office of Energy Research, Office of Basic Energy Sciences, Chemical Sciences Division, of the U.S. Department of Energy under Contract No. DE-AC02-05CH11231. R. M. R. would like to acknowledge the Ford Motor Company for financial support through a graduate fellowship administered by the Berkeley Catalysis Center. The authors would also like to thank Mr. Gabor London for his assistance with compiling literature on low temperature selective catalytic reactions.

References

- [1] M. Boudart, *J. Mol. Catal.* 30 (1985) 27.
- [2] M.J. Yacamán, S. Fuentes and J.M. Dominguez, *Surf. Sci.* 106 (1981) 472.
- [3] M. Gillet and A. Renou, *Surf. Sci.* 90 (1979) 91.
- [4] B. Coq and F. Figueras, *Coord. Chem. Rev.* 178–180 (1998) 1753.
- [5] A.S. McLeod and L.F. Gladden, *J. Catal.* 173 (1998) 43.
- [6] L.F. Gracia and E.E. Wolf, *Chem. Eng. J.* 82 (2001) 291.
- [7] R. Van Hardeveld and F. Hartog, *Surf. Sci.* 15 (1969) 189.
- [8] S. Ladas, *Surf. Sci.* 175 (1986) L681.
- [9] R.B. Greegor and F.W. Lytle, *J. Catal.* 63 (1980) 476.
- [10] J.J. Burton, *Catal. Rev.* 9 (1974) 209.
- [11] M. Mavrikakis, M. Bäumer, H.J. Freund and J.K. Nørskov, *Catal. Lett.* 81 (2002) 153.
- [12] M. Boudart, *Adv. Catal.* 20 (1969) 153.
- [13] M. Boudart, *Top. Catal.* 13 (2000) 147.
- [14] H. Lang, R.A. May, B.L. Iverson and B.D. Chandler, *J. Am. Chem. Soc.* 125 (2003) 14832.
- [15] R.M. Rioux, H. Song, J.D. Hoefelmeyer, P. Yang and G.A. Somorjai, *J. Phys. Chem. B* 109 (2005) 2192.
- [16] J.W. Yoo, D.J. Hathcock and M.A. El-Sayed, *J. Catal.* 214 (2003) 1.
- [17] J.W. Yoo, D. Hathcock and M.A. El-Sayed, *J. Phys. Chem. A* 106 (2002) 2049.
- [18] Z. Kónya, V.F. Puentes, I. Kiricsi, J. Zhu, A.P. Alivisatos and G.A. Somorjai, *Catal. Lett.* 81 (2002) 137.
- [19] Z. Kónya, V.F. Puentes, I. Kiricsi, J. Zhu, A.P. Alivisatos and G.A. Somorjai, *Nano. Lett.* 2 (2002) 907.
- [20] Z. Kónya, V.F. Puentes, I. Kiricsi, J. Zhu, J.W. Ager III, M.K. Ko, H. Frei, A.P. Alivisatos and G.A. Somorjai, *Chem. Mater.* 15 (2003) 1242.
- [21] J. Zhu, Z. Kónya, V.F. Puentes, I. Kiricsi, C.X. Miao, J.W. Ager III, A.P. Alivisatos and G.A. Somorjai, *Langmuir* 19 (2003) 4396.
- [22] B. Wiley, Y. Sun, B. Mayers and Y. Xia, *Chem. Eur. J.* 11 (2005) 454.
- [23] J. Chen, T. Herricks, M. Geissler and Y. Xia, *J. Am. Chem. Soc.* 126 (2004) 10854.
- [24] T.J. Herricks, J. Chen and Y. Xia, *Nano Lett.* 4 (2004) 2367.
- [25] X. Teng and H. Yang, *Nano. Lett.* 5 (2005) 885.
- [26] Y.-W. Jun, J.-H. Lee, J.S. Choi and J. Cheon, *J. Phys. Chem. B* 109 (2005) 14795.

- [27] H. Song, F. Kim, S. Connor, G.A. Somorjai and P. Yang, *J. Phys. Chem. B* 109 (2005) 188.
- [28] H. Song, R.M. Rioux, J.D. Hoefelmeyer, R. Komor, K. Niesz, M. Grass, P. Yang and G.A. Somorjai, Submitted to *J. Am. Chem. Soc.* 128 (2006) 3027.
- [29] R.M. Rioux, T.J. Toops, M. Grass, K. Niesz, H. Song, R.M. Rioux, P. Yang and G.A. Somorjai, Submitted to *Chem. Mater.* (2006).
- [30] W.A. Dietz, *J. Gas. Chrom.* 5 (1967) 68.
- [31] R.J. Madon and M. Boudart, *Ind. Engr. Chem. Fund.* 21 (1982) 438.
- [32] R. Yu, H. Song, X.-F. Zhang and P. Yang, *J. Phys. Chem. B* 109 (2005) 6940.
- [33] F. Zaera and G.A. Somorjai, *J. Am. Chem. Soc.* 106 (1984) 2288.
- [34] A.L. Backman and R.I. Masel, *J. Vac. Sci. Technol. A* 6 (1988) 1137.
- [35] L.P. Ford, H.L. Nigg, P. Blowers and R.I. Masel, *J. Catal.* 179 (1988) 163.
- [36] J. Grunes, J. Zhu, E.A. Anderson and G.A. Somorjai, *J. Phys. Chem. B* 106 (2002) 11463.
- [37] A.M. Contreras, J. Grunes, X.-M. Yan, A. Liddle and G.A. Somorjai, *Catal. Lett.* 100 (2005) 115.
- [38] T.A. Dorling, M.J. Eastlake and R.L. Moss, *J. Catal.* 14 (1969) 23.
- [39] J.C. Schlatter and M. Boudart, *J. Catal.* 24 (1972) 482.
- [40] V.B. Kazanskii and V.P. Strunin, *Kinet. Katal.* 1 (1960) 553.
- [41] R.D. Cortright, S.A. Goddard, J.E. Rekoske and J.A. Dumesic, *J. Catal.* 127 (1991) 342.
- [42] H. Ewald, A.A. Shestov and V.S. Muzykantov, *Catal. Lett.* 25 (1994) 149.
- [43] H. Imamura, M. Yoshinobu, T. Mihara, Y. Sakata and S. Tsuchiya, *J. Mol. Catal.* 69 (1991) 271.
- [44] V.Y. Borovkov, D.R. Luebke, V.I. Kovalchuk and J.L. d'Itri, *J. Phys. Chem. B* 107 (2003) 5568.
- [45] V.I. Avdeev, V.I. Kovalchuk, G.M. Zhidomirov and J.L. d'Itri, *Surf. Sci.* 583 (2005) 46.
- [46] R. Camprostrini, G. Caruran and R.M. Baraka, *J. Mol. Catal.* 78 (1993) 169.
- [47] K.P. De Jong, B.E. Bongenaar-Schlenter, G.R. Meima, R.C. Verkerk, M.J.J. Lammers and J.W. Geus, *J. Catal.* 81 (1983) 67.
- [48] M. Hansen, *Constitution of Binary Alloys*, (McGraw-Hill, New York, 1958).
- [49] D. Lahiri, B. Bunker, B. Mishra, Z. Zhang, D. Meisel, C.M. Doudna, M.F. Bertino, F.D. Blum, A.T. Tokuhito, S. Chattopadhyay, T. Shibata and J. Terry, *J. Appl. Phys.* 97 (2005) 094304.
- [50] U. Strüber, A. Kastner and J. Küppers, *Thin Solid Films* 250 (1994) 101.
- [51] H. Röder, R. Schuster, H. Brune and K. Kern, *Phys. Rev. Lett.* 71 (1993) 2086.
- [52] P. Claus, *Top. Catal.* 5 (1998) 51.
- [53] M.A. Englisch, A. Jentys and J.A. Lercher, *J. Catal.* 166 (1997) 25.
- [54] G.F. Santori, M.L. Casella, G.J. Siri, H.R. Adúriz and O.A. Ferretti, *React. Kinet. Catal. Lett.* 75 (2002) 225.
- [55] M.A. Vannice and B. Sen, *J. Catal.* 115 (1989) 65.
- [56] T. Birchem, C.M. Pradier, Y. Berthier and G. Cordier, *J. Catal.* 146 (1994) 503.
- [57] C.M. Pradier, T. Birchem, Y. Berthier and G. Cordier, *Catal. Lett.* 29 (1994) 371.
- [58] F. Delbecq and P. Sautet, *J. Catal.* 152 (1995) 217.
- [59] F. Delbecq and P. Sautet, *J. Catal.* 211 (2002) 398.
- [60] A. Giror-Fendler, D. Richard and P. Gallezot, *Catal. Lett.* 5 (1990) 175.
- [61] M. Lashdaf, J. Lahtinen, M. Lindblad, T. Venäläinen and A.O.I. Krause, *Appl. Catal. A Gen.* 276 (2004) 129.